Journal of Marine Research, 62, 663–683, 2004

Oxygen variability in the near-surface waters of the northern North Atlantic: Observations and a model

by Peter Lazarevich[1], Tom Rossby[2] and Craig McNeil[2]

ABSTRACT

As part of the World Ocean Circulation Experiment a major study was undertaken to determine the absolute circulation of the Subpolar North Atlantic using a large number of acoustically tracked isopycnal floats deployed on the 27.5 σ_θ surface. Fifty floats were equipped with sensors to study dissolved oxygen from a Lagrangian perspective. In this paper we comment on very large variations in oxygen along trajectories of fluid parcels that outcrop in winter and resubduct the following spring. We employ a one-dimensional model to interpret these in terms of biophysical processes at and near the surface.

In an attempt to understand the observed variability, we find that a modified form of the Price-Weller-Pinkel mixed layer model using NCEP-derived surface forcing accurately reproduces both the float-observed temperature and the meteorological-based sea-surface temperatures to within 1°C for an entire year, including the timing of the ventilation and restratification observed by the float. The model also employs satellite-derived observations to represent three processes of oxygen exchange: an air-sea gas flux dependent upon wind-driven turbulence, oxygen production in the mixed layer as a result from primary productivity, and oxygen consumption at depth as a result of net community respiration. The model accurately reproduces the observed ~3% supersaturation in the wintertime mixed layer, a level which is supported by the air-sea gas flux. We also find that later in the year, during springtime restratification, the model reproduces the observed decline from 105% to 92% oxygen saturation.

The good agreement between observation and model depends upon a one-dimensional balance in the vertical, i.e. the absence of horizontal advective effects. For floats outcropping in an area of horizontal thermal contrast, conspicuous errors in the predicted vertical structure arise, most likely due to horizontal advection or displacement of the float by surface winds, effects which cannot be assessed without additional information. This limitation notwithstanding, the agreement between model and observation indicates the power of Lagrangian techniques for understanding how the properties of surface waters are set and later modified as they subduct into the interior of the ocean.

1. Introduction

The variability of near-surface waters is of great interest to oceanographers. It is at the surface that most water-transformation occurs, driven not only by heat and salt exchanges,

1. Department of Oceanography, Florida State University, Tallahassee, Florida, 32306-4320, U.S.A. ***email: plazarev@fsu.edu***

2. Graduate School of Oceanography, University of Rhode Island, Narragansett, Rhode Island, 02882, U.S.A.

but also by air-sea and biologically-related gas exchanges. Additionally, waters that subduct from the surface can spread out over great horizontal distances and substantially alter the large-scale distribution. Given that the surface is the only active boundary of the ocean, it behooves the oceanographer to understand the underlying processes controlling the observed vertical structure of near-surface waters. In particular, with biogenic gases such as oxygen, the major difficulty we face is quantifying the relative roles of air-sea and biologically-related fluxes.

Numerous studies of oxygen variability in near-surface waters have clearly shown that the air-sea flux is primarily dependent upon wind-generated oceanic turbulence. These include Thorpe (1984), Woolf and Thorpe (1991), Wallace and Wirick (1992), Farmer *et al.* (1993), and Wanninkhof and McGillis (1999). These studies link the enhanced gas transfer rates found at high wind speeds to crashing waves and the injection of air bubbles to depths of several meters and dissolution of micro-bubbles transported within Langmuir circulation cells to depths of tens of meters. Bubbles provide a greater surface area for air-sea exchange and, since they are at slightly elevated pressures when below the surface, provide a mechanism for the supersaturation of near-surface waters. The most recent of these studies suggests a cubic relationship between air-sea gas exchange and wind speed. Fortunately, wind speed is now remotely sensed which makes it a readily available parameter with which to estimate an air-sea gas exchange.

Biologically-driven oxygen fluxes are more difficult to estimate. The two main processes are oxygen production in the mixed layer via primary productivity and oxygen consumption at depth via net community respiration. Both of these are time and depth dependent and are often difficult to measure directly. An alternate approach to direct measurement is to back-out the oxygen production by using remotely-sensed estimates of primary productivity, such as that from the Vertically Generalized Production Model (VGPM) (Behrenfeld and Falkowski, 1997). Their model uses satellite-derived chlorophyll concentrations to obtain primary productivity rates for the world's oceans. A dataset such as theirs can now serve as a globally-available quantity to estimate biologically-driven oxygen fluxes.

In this paper we present direct, Lagrangian float observations of pressure, temperature, and oxygen in the near-surface waters of the northern North Atlantic from the winter of 1998 through the fall of 1999. These isopycnal floats, representing a subset of floats ballasted for the 27.5 σ_θ density surface, are of particular interest because they outcrop into the wintertime mixed layer and subduct during springtime restratification. They constitute a unique data set with which to explore our understanding of processes that govern dissolved oxygen as waters surface and subduct throughout the seasonal cycle. With this information in hand, we attempt to model the observed variability using meteorological and bio-optical observations that act upon climatologically-derived vertical profiles of temperature, salinity, and oxygen in the upper 700 m of the water column. The model output or prediction of temperature is compared to the float observations to determine the appropriateness of our one-dimensional, vertical model. The oxygen variability is dis-

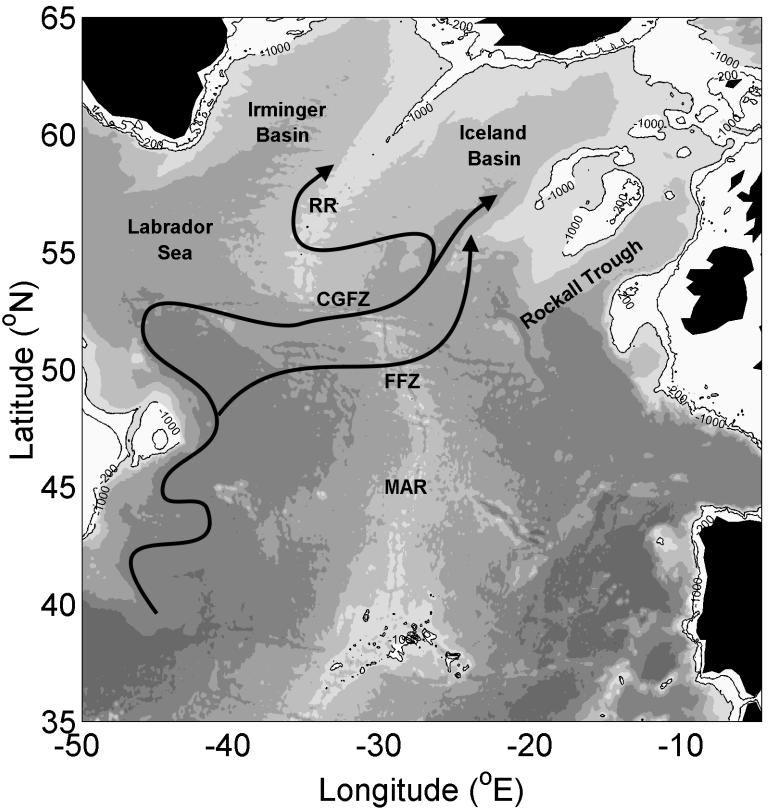

Figure 1. The study area showing the primary warm-water pathways (arrows), major basins, and the following topographic features: Reykjanes Ridge (RR), Charlie Gibbs Fracture Zone (CGFZ), Faraday Fracture Zone (FFZ), and the Mid-Atlantic Ridge (MAR). Floats were deployed along the north-south line at 37W.

cussed in detail, with special attention given to the interdependence of the air-sea and biological fluxes.

2. Study area

Our region of interest is the Subpolar North Atlantic (Fig. 1). The general circulation is dominated by the North Atlantic Current, which carries old and nutrient-rich, subtropical-origin waters. They flow northward east of the continental shelf of Newfoundland in the western North Atlantic as far north as 50N to 52N, where, at the Northwest Corner, they abruptly turn to the east and head toward the Mid-Atlantic Ridge. These waters, flowing eastward as part of the Subpolar Front, cross the ridge preferentially through the Charlie-Gibbs Fracture Zone and Faraday Fracture Zone and into the eastern North Atlantic. Once past the ridge, these waters flow northeast into the Iceland Basin or

retroflect back to the west and enter the Irminger Basin (Pérez-Brunius *et al.,* 2004; Bower *et al.,* 2002). At these high latitudes, i.e., north of 54N in the Irminger Basin and Labrador Sea, the 27.5 σ_θ density surface can outcrop into the wintertime mixed layer. When these waters outcrop, they replenish the nutrient levels in the mixed layer that were consumed the previous year and set the stage for a relatively intense bloom later in the year. Later, during the springtime, surface waters restratify and the 27.5 σ_θ density surface subducts as modified Subpolar Front waters.

3. Float observations

During 1997–2000, our group participated in the Atlantic Climate Change Experiment, a major field study of the Subpolar North Atlantic (Molinari *et al.,* 1994). We tracked 50 isopycnal RAFOS floats in an effort to determine the absolute velocity field (Bower *et al.,* 2002). Additionally, these were the first RAFOS floats to measure oxygen. This was an exploratory effort to evaluate the feasibility of measuring oxygen along isopycnal float trajectories and to understand the processes responsible for the observed variations. By and large the results were very encouraging. We used a YSI-5750 polarographic sensor operating in the pulsed mode (Langdon, 1986). See Appendix for further details about the RAFOS float operation and oxygen measurements.

Of the 50 floats tracked, six floats outcropped into the wintertime mixed layer and subducted the following spring. In doing so they evidenced very large oxygen variations. In this paper, we focus on two floats, #540 and #550, which are representative of the six floats. Figure 2 shows the portions of their tracks which were used in the following analyses. Since these floats spent almost an entire year near the surface, shallower than 200 m, they observed strong seasonal variability. Because the floats drift with the waters, we shall invoke the oft-used assumption that the local balances do not involve horizontal advection but only vertical variations, i.e. we restrict ourselves to a vertical, one-dimensional model. The question then becomes, how well can we interpret and explain the observed variations in temperature and oxygen along the trajectories.

4. Model

Our model is based upon the Price, Weller, Pinkel (PWP) ocean model (Price *et al.,* 1986). It is a vertical, one-dimensional model that tracks the evolution of temperature and salinity profiles under a prescribed set of meteorological conditions. The PWP model is well suited for determining mixed layer depths in extra-tropical waters during wintertime convection, as demonstrated by Plueddemann *et al.* (1995). We have supplemented the original code with the ability to track the evolution of oxygen profiles (see our website for information about our model: http://www.po.gso.uri.edu/rafos/research/pwp/index.html). The model is run with initial profiles determined from climatology and driven with daily averages of meteorological and gas fluxes evaluated at the float's location. The initial profiles are discussed in Section 4a, the meteorological fluxes in Section 4b, and the oxygen fluxes in Sections 4c and 4d.

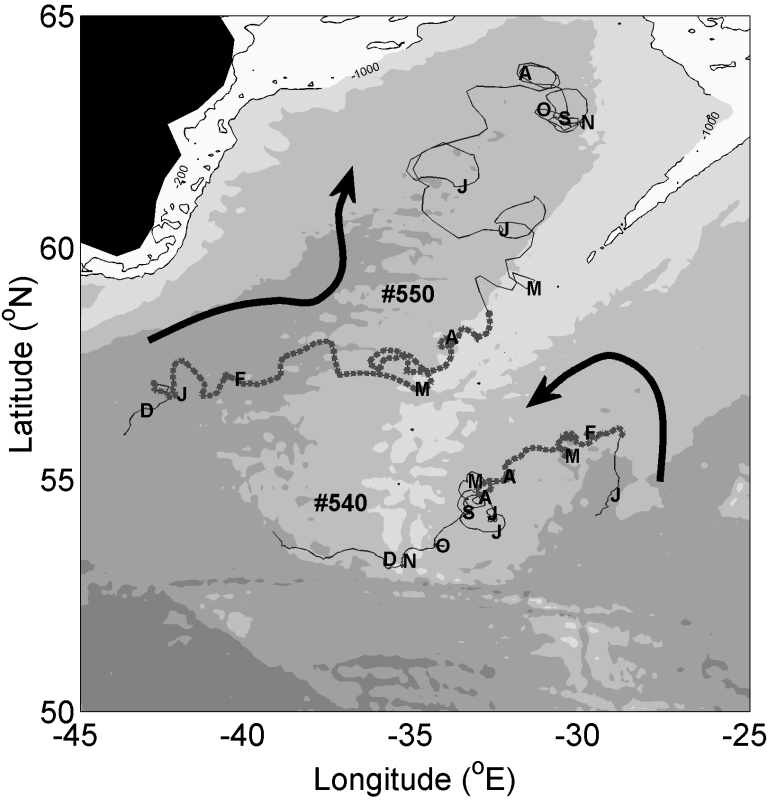

Figure 2. Portions of float tracks for RAFOS floats #540 and #550. The month of the year is indicated with the text labels along the tracks and the dots indicate the time when the floats are in the wintertime mixed layer. Direction of motion is indicated by the arrows.

a. Initial profiles

Initial profiles of temperature, salinity, and oxygen were obtained using an analysis of historical hydrography for the region. The temperature and salinity profiles were estimated through a monthly-averaged Gravest Empirical Mode (GEM) analysis (Pérez-Brunius *et al.,* 2004). The GEM technique yields the most representative profile that matches the float's temperature and pressure as well as its density; for a complete discussion of the GEM technique, see Sun and Watts (2001). Unfortunately, the number of wintertime observations of oxygen in the climatology was too sparse for a monthly GEM analysis. Instead, we simply averaged the wintertime (December through February) oxygen profiles for our region of interest. Figure 3 shows the mean profiles for the model run of float #540. The standard deviation of the mean is also shown and represents the variability in the climatological fields.

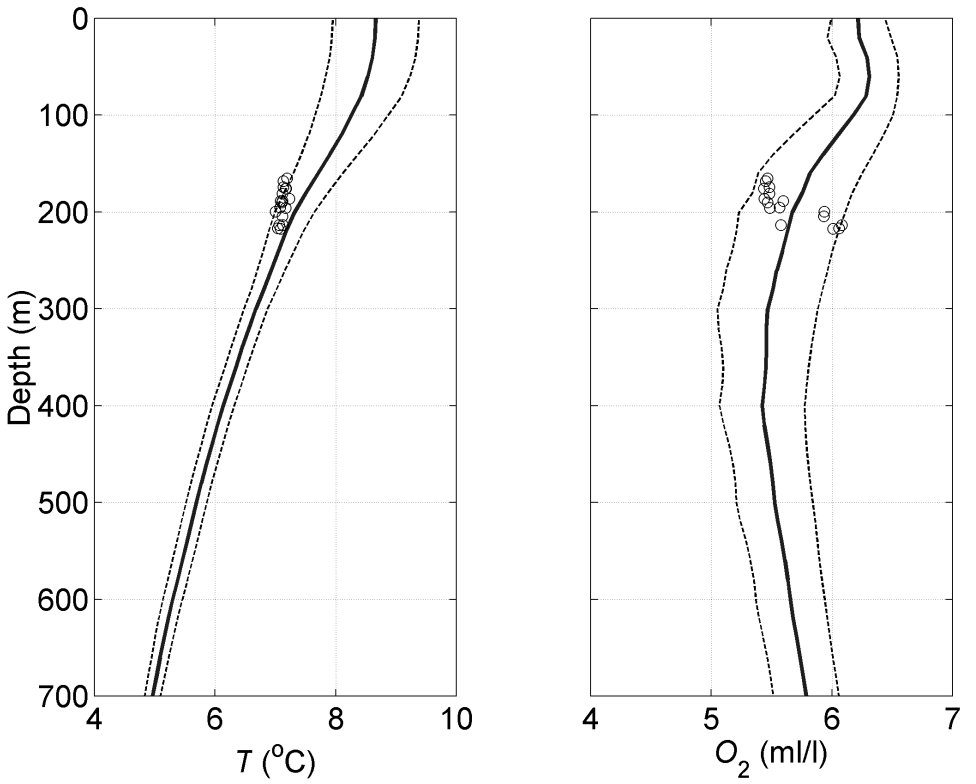

Figure 3. Initial temperature (T) and oxygen (O_2) profiles (solid lines) for the model run of float #540. The dashed lines represent the standard deviations from the climatological averaging. Also shown are the float observations corresponding to the first 20 days of the model run.

b. Meteorological fluxes

The model is forced with daily-averages of meteorological fluxes using data from the NCEP/NCAR Reanalysis CD-ROM (Kistler *et al.,* 2001). These fluxes are analyzed fields with daily averaging and a horizontal resolution of about 25 km; specifically, these are not climatological averages. The model requires the following inputs, all available on the CD-ROM: net short-wave radiation, net long-wave radiation, latent heat, sensible heat, precipitation, north-south and east-west wind stresses, and north-south and east-west wind speeds at 10 m.

c. Oxygen fluxes—physical processes

The key modification we made to the PWP model was to include estimates of oxygen fluxes from both physical and biological processes. The dominant physical process is the air-sea flux associated with bubble injection. This is a flux whose rate and equilibrium

point are functions of wind-generated turbulence. Both aspects can be parameterized in terms of wind speed, using the bulk formula from Woolf and Thorpe (1991):

$$F_{air} = K_T[C_{sat}(1 + \Delta e) - C_{ml}] \tag{1}$$

where F_{air} is the air-sea gas flux of oxygen, K_T is the transfer velocity (in units of m/s), C_{sat} and C_{ml} are the oxygen concentrations at saturation and in the mixed layer, respectively, and Δe is the equilibrium fractional supersaturation and determines the equilibrium saturation point. K_T is also referred to as the piston velocity and can be used to estimate an e-folding time constant, τ, for a mixed layer of depth, h, to reach gas equilibrium with the atmosphere:

$$\tau \sim h/K_T. \tag{2}$$

Both K_T and Δe have previously been expressed as functions of the wind speed at 10 m, W_{10}. For K_T, we use the cubic relation established by Wanninkhof and McGillis (1999):

$$K_T = \alpha(W_{10})^3 \tag{3}$$

where the proportionality constant, α, is gas-species dependent, and, for oxygen, is approximately 7.0×10^{-8} (for K_T and W_{10} in m/s). For Δe, we use the quadratic relation of Woolf and Thorpe (1991):

$$\Delta e = 0.01\left(\frac{W_{10}}{9}\right)^2 \tag{4}$$

with W_{10} in m/s. The final expression, which is parameterized in terms of wind speed only, is:

$$F_{air} = 7 \times 10^{-8}(W_{10})^3\left(C_{sat}\left(1 + 0.01\left(\frac{W_{10}}{9}\right)^2\right) - C_{ml}\right). \tag{5}$$

The combined wind speed dependence of (5) represents an upper limit within the available literature.

d. Oxygen fluxes—biological processes

Next, we attempt to estimate the oxygen flux from two key biological processes: primary productivity near the surface and net community respiration at depth. Here, we use the primary productivity estimates from the Vertically Generalized Production Model to back-out the fluxes. First, the primary productivity, PP_{eu}, (in $gC/m^2/day$) is converted to an oxygen production rate, F_{PP}, (in $molO_2/m^2/day$) using a photosynthetic quotient, PQ, of 1.2 (Kirk, 1983):

$$F_{PP} = PP_{eu} \cdot \frac{1\text{molCO}_2}{12\text{gC}} \cdot \underbrace{\frac{1.2\text{molO}_2}{1\text{molCO}_2}}_{PQ} \tag{6}$$

where PQ is defined as the molar ratio of oxygen produced to carbon fixed. This production is assumed to be uniformly distributed and entirely confined to the mixed layer. Thus, the model cannot recreate a subsurface oxygen maximum, a feature typically observed in the late summer (Najjar and Keeling, 1997).

Finally, we use the f ratio to relate PP_{eu} to the net community respiration rate, R, and the associated oxygen consumption rate, F_R:

$$R = f \cdot PP_{eu} \Rightarrow F_R \tag{7}$$

where the arrow represents a change in units, from $gC/m^2/day$ to $molO_2/m^2/day$, as shown in (6). Documented values for f range from 0.15 to 0.45. The most recent studies suggest that ratios at the high-end of the range may be more realistic (Mann and Lazier, 1996; Najjar and Keeling, 2000). Here, we use a value of 0.25.

Using the three oxygen fluxes: F_{air}, F_{PP}, and F_R, we now have sufficient model inputs to calculate the resulting changes in oxygen concentration. This last step requires us to estimate the volume, i.e. depth, over which these fluxes are distributed. For F_{air} and F_{PP}, the appropriate depth-scale is the mixed layer depth, Z_{ml}:

$$\Delta C_{ml} = \frac{F_{air} + F_{PP}}{Z_{ml}} \tag{8}$$

where ΔC_{ml} is the daily change in oxygen concentration in the mixed layer. For F_R, the appropriate depth-scale is not so clearly defined. We can, however, make use of typical sinking rates for phytoplankton cells, ~1 m/day, and the time-scale for their remineralization, ~100 days (Smayda, 1970; Fowler and Knauer, 1988). Their product results in a depth-scale for F_R of ~100 m and thus the change in oxygen concentration for the remineralization zone (the first 100 m below the mixed layer) is:

$$\Delta C_R = \frac{F_R}{100}. \tag{9}$$

These fluxes and their associated concentration changes are shown in Figure 4.

e. Steps

The modified-PWP model has the following five steps:

1) *Apply daily-averaged air-sea fluxes of heat, salt, and the oxygen fluxes.* The incoming, short-wave heat flux is absorbed at depth using a two-component exponential while the other heat fluxes (long-wave, latent, and sensible) are applied directly at the surface. The salt flux, in reality a freshwater flux, is simply the difference between evaporation and precipitation and is applied at the surface. Additionally, F_{air} and F_{PP} are applied at the surface while F_R is applied evenly with the first 100 m below the mixed layer.

2) *Remove any static instability in the density profile.* Surface waters are mixed to

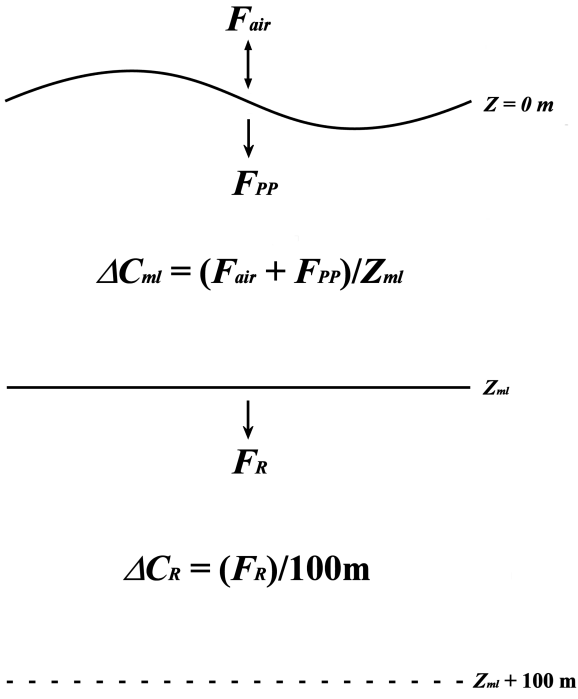

Figure 4. Schematic of the oxygen fluxes and their corresponding daily concentration changes. All fluxes are applied uniformly within either the mixed layer (F_{air} and F_{PP}) or the first 100 m below the base of the mixed layer (F_R).

increasing depth until the density profile becomes statically-stable again. This process represents free convection and also homogenizes temperature, salinity, and oxygen.

3) *Calculate the depth of the mixed layer.* The depth of the mixed layer is found to be the depth at which density first begins to increase.

4) *Apply the daily-averaged air-sea momentum flux.* The momentum transfer from the surface wind stress is applied uniformly to the entire mixed layer. Also at this time, the velocity profile is rotated by an angle determined by the inertial period and time step of the model.

5) *Perform Richardson instability mixing.* First, the bulk Richardson instability criterion is tested and the mixed layer is incrementally deepened until the criterion is met. Next, gradient Richardson mixing takes place if the velocity gradient at the base of the mixed layer is too high. This second step only smoothens the transition at the base of the mixed layer and does not deepen it.

6) *Apply vertical diffusion to the profiles.* A small amount of vertical diffusion,

$O(10^{-5})$ m^2/s is applied. This form of mixing is most important during the spring and summer, when strong and sharp vertical gradients in temperature develop at the surface.

5. Results

a. Physics

The model output is compared to the pressure and temperature measurements of the float, as shown in Figure 5. In each panel, the outcropping period is indicated along the bottom by the solid bar. In the upper panel, we compare the mixed layer depth of the model (solid line) to the float pressure (dots). Note that the float rapidly shoals in late January, 1999 which indicates that the float has outcropped into the wintertime mixed layer. The model accurately predicts the timing of this outcropping, as the mixed layer depth reaches the float's depth at the appropriate time. Note how, from late January to March, the float slowly rises to the surface. This reflects the fact that the float was designed with a compressee that has a limited operating range, and at these shallow depths the float is behaving isobarically instead of isopycnally. By March, the float has become completely buoyant and starts to 'bob' up and down from the surface. These vertical excursions can be quite large, $O(100)$ m. Later, in mid-April, the float's pressure becomes more stable, indicating the initiation of stratification. The model also predicts restratification at this time, as the mixed layer depth decreases from 300 m to 50 m. From then until September, the model predicts a shallow, ~20 m deep mixed layer that is at all times shallower than the float as it subducts from about 50 m to 130 m. In December, the float outcrops once again, at a time for which the model predicts a deepening mixed layer.

In the second panel, we compare the model temperature (solid line) at the float's depth to the float temperature (dots). During the outcropping period, both show a similar initial drop. Once restratification begins, the two track a similar increase until August, by which time the model is ~0.5°C colder than the float. The third panel shows the model density (solid line) at the float's depth and the assumed float's density (dots—the flat line). The float's density represents our best estimate of the float's ballasting at the time of deployment in July, 1998. For this float, its ballast density was 27.32 σ_θ, instead of the 27.5 σ_θ as we had intended. During the outcropping period, the model correctly predicts a slow densification of the mixed layer followed by a relatively rapid drop back to the original density before outcropping.

As an additional model check, we compare the sea-surface temperature (SST) of the model (solid line) to the NCEP reanalysis SST (dashed line) in the third panel. At most times, they are within 1°C of each other, a rather remarkable agreement for a year-long time series. Furthermore, the timing of maximum SST is off by only three weeks. Finally, we show the net heat flux in the lower panel, where positive values represent heat gain by the ocean. As expected, a net heat loss is associated with the deepening of the mixed layer and a net heat gain (from April to September) is associated with increasing SST.

To summarize, the main result here is that the model appears to work quite well. It

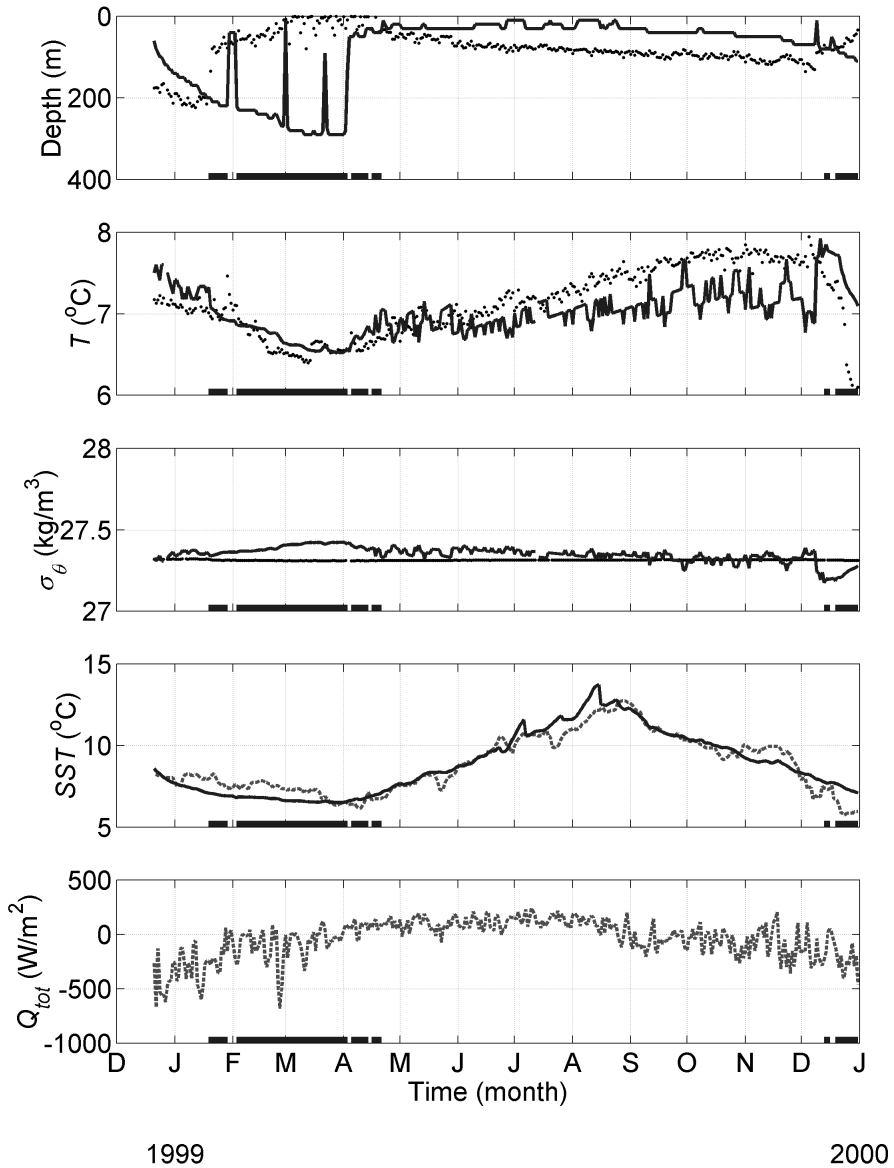

Figure 5. Model output (solid line) and float observations (dots) of pressure (depth), temperature (T), and potential density (σ_θ) for float #540. Also shown are the NCEP reanalysis products (dashed lines) of sea-surface temperature (SST) and net heat flux (Q_{tot}).

accurately predicts temperature at two points in the vertical: at the float's depth and at the surface. Also, the timing of the outcropping and restratification are correctly predicted. The model's performance with regard to these two points is a clear indication that the observed

variability is a result of vertical, and not horizontal, processes. By using RAFOS floats, we have removed a substantial amount of variability from advection that would otherwise be present in stationary, Eulerian observations.

b. Biology

The model tracks very well the float oxygen measurements, as shown in Figure 6. Both show a similar increase just as the float outcrops, going from about 85% saturation to just over 100% saturation. During the outcropping period, there is a slight increase from 100% to 105% saturation. As the float begins to subduct, the oxygen drops at an initial rate of 5% per month, down to 92% after four months. The second and third panels show F_{air} and F_{PP}, respectively. Since F_{air} is strongly dependent upon W_{10} and F_{PP}, is directly related to PP_{eu}, they are also shown in the two lower panels. The large peaks in F_{air} are associated with peaks in W_{10} *and* a deepening mixed layer, since stronger storms and the entrainment of relatively low-oxygen waters both act to increase the flux gradient across the air-sea interface. When the waters become stratified, F_{PP} increases and leads to a supersaturation of the mixed layer. Consequently, F_{air} reverses sign as the mixed layer must now expel oxygen to reach gas equilibrium. As the float continues to subduct away from the mixed layer, both F_{PP} and F_R (not shown) become large. It is F_R, directly proportional to F_{PP}, which is responsible for the observed O_2 drawdown at depth. By the end of September the surface productivity has died down and at the same time the oxygen drawdown ceases.

6. Discussion

a. Air-sea fluxes versus biogenic fluxes

There is a remarkable agreement between the float and model oxygen. Of special interest is the ability of the model to reproduce the oxygen drawdown at depth that begins in May. The only mechanism that the model has to reproduce this drop is via net community respiration, as demonstrated in Figure 7. Here, we show the model output for two test cases: (1) with F_{air} alone and (2) with F_{air} and F_{PP}, and compare them to the full model output with all the fluxes included: (3) F_{air}, F_{PP}, and F_R. Initially, the three model runs and the float are all in agreement, showing a similar, 5% increase in oxygen during the outcropping period. This is at a time when there is little biological activity and the dominant flux is F_{air}. When restratification occurs, the float leaves the mixed layer and the oxygen starts to drop. As shown in the top panel, the oxygen from the test cases (1) and (2) remains slightly above saturation for the remainder of the model run. The oxygen from the model run for (2) is slightly higher due to additional flux from F_{PP} while the float was outcropped in late April. The only process that can recreate the observed oxygen drop is via a net community respiration, as shown with the model run for (3). For completeness, we also show the surface value of oxygen in the lower panel. Note that the biological activity has a rapid and pronounced effect at the surface.

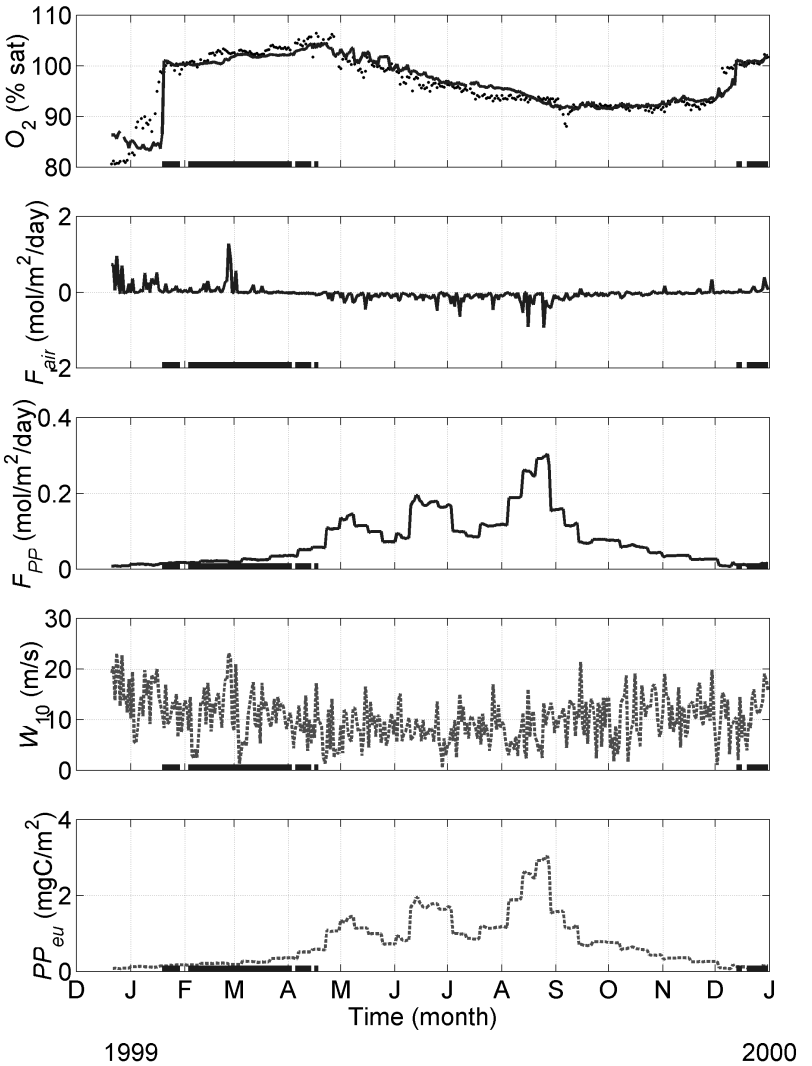

Figure 6. Model output (solid line) and float observations (dots) of oxygen (O_2) for float #540. Also shown are the modeled oxygen fluxes (F_{air} and F_{PP}). The two lower panels show the NCEP reanalysis product of the wind speed (W_{10}) and the VGPM product of primary productivity (PP_{eu}).

Next, we diagnose the impact that the biological flux, F_{PP}, has upon the air-sea flux, F_{air}, as shown in Figure 8. Here we show F_{air} for two model runs: the top panel is from the model run with F_{air} alone and the second panel is for the full model run, F_{air}, F_{PP}, and F_R. In the top panel, F_{air} is large during the wintertime when the mixed layer is deep and storm activity is high. During the spring and summer the mixed layer

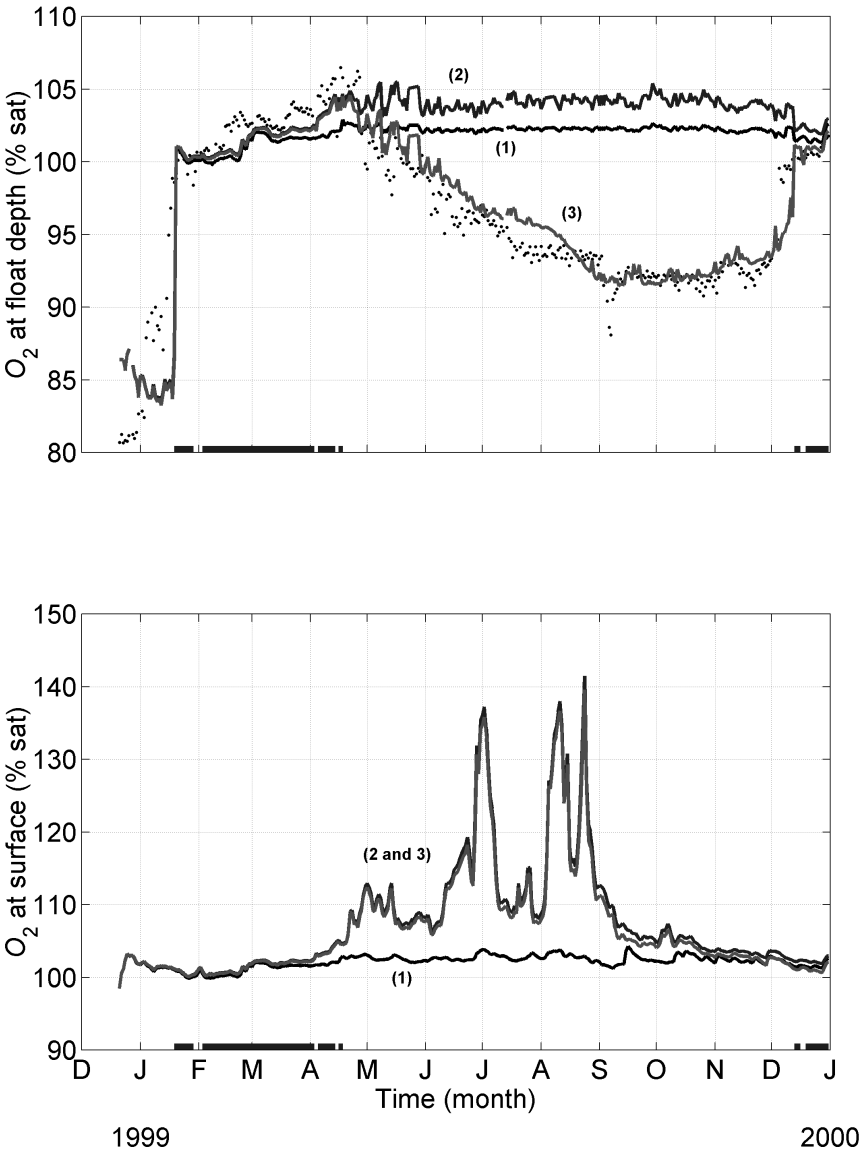

Figure 7. Model oxygen (O_2) from three different runs for float #540. The labels refer to model runs with: (1) air-sea flux alone, (2) air-sea flux and primary productivity, and (3) air-sea flux, primary productivity, and respiration.

shallows and, since a smaller flux is required to maintain gas equilibrium, F_{air} becomes quite small. In the middle panel, F_{air} becomes quite large from late April to early June, when the primary productivity is highest. Since primary productivity acts as a positive

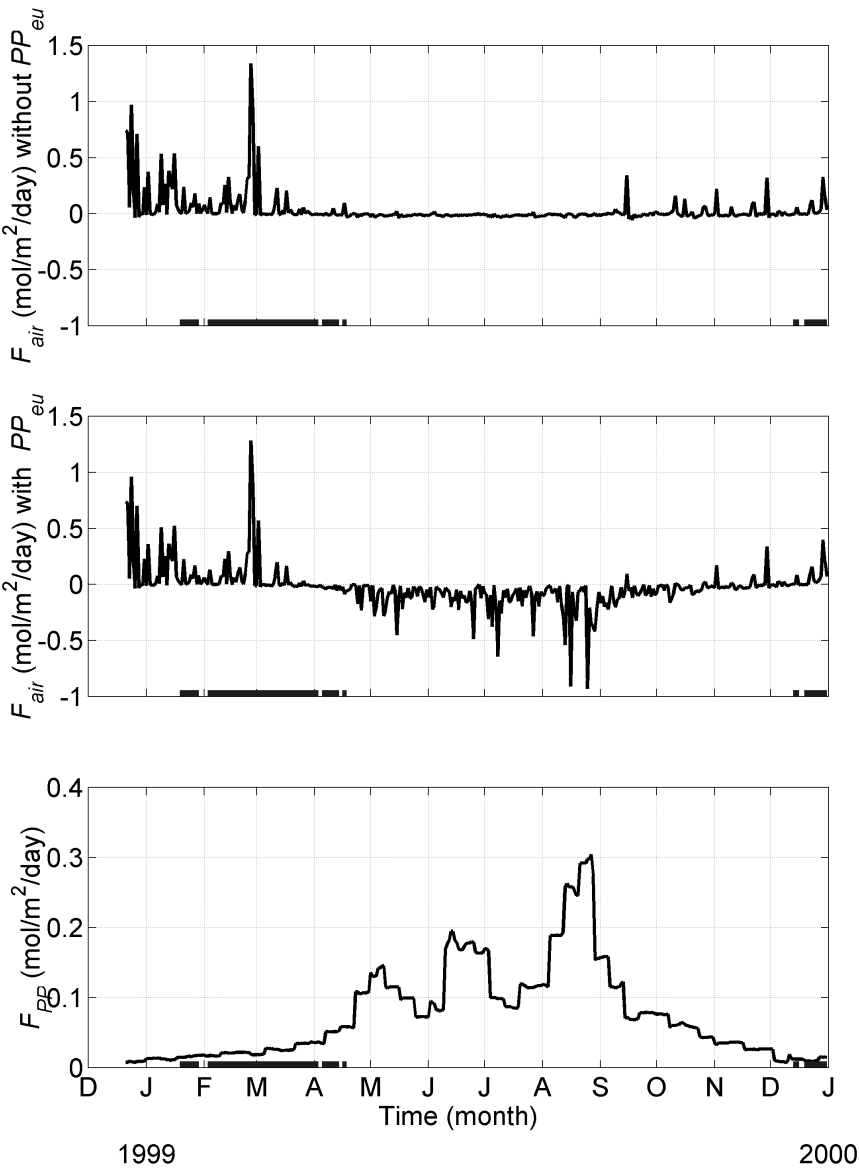

Figure 8. Model oxygen fluxes for two different runs for float #540. The top panel is with F_{air} alone and the middle panel is with all three fluxes: F_{air}, F_{PP}, and F_R. The bottom panel shows F_{PP}.

oxygen supply into the mixed layer, the model compensates by degassing oxygen from the mixed layer to the atmosphere. This is a noteworthy result, showing how the biological flux impacts the air-sea flux. For completeness, we show F_{PP} in the lower panel.

b. Limitations of the model

In contrast to the model results from float #540, we now present a case where the model is unable to account for the observed variability, float #550. Figure 9 shows the model and float pressure, temperature, and potential density (σ_θ). The model is still able to predict the timing of outcropping and restratification. However, from February to March and then from April to May, the float reveals large, 1°C, increases in temperature. The model is completely unable to reproduce these jumps, since the dominant control of temperature is the net heat loss at the surface. In fact, the NCEP reanalysis suggests a substantial, $\sim$300 W/m^2 heat loss during the first jump. Undoubtedly, these jumps are not associated with a heat gain at the surface but must be a result of lateral mixing. In support of this conclusion, these jumps take place as the float is drifting eastward and toward the warmer waters from the SPF over the Reykjanes Ridge (Fig. 1). Also, note that the model SST is lower than the observed SST by about 2°C which further implicates lateral mixing with warmer waters.

The model's performance for oxygen is just as poor. In Figure 10, the float shows low-oxygen spikes which the model is not able to reproduce. These spikes occur simultaneously with the initiation of stratification, and just prior to the second temperature increase in mid April. This suggests that the float is crossing through a front, which might have a substantial amount of stratification associated with it. If that is the case, the enhanced stratification would intensify the net community respiration, resulting in the large, downward oxygen spikes in April.

A close examination of oxygen in Figure 7 and Figure 10 indicate a larger scatter toward lower values of oxygen, especially in springtime very soon after the seasonal thermocline begins to establish itself. This shows up in other float oxygen records as well. We do not have a specific explanation for these events, but suspect that they reflect very local drawdowns in oxygen where particulate matter aggregates on thin strata. Since there is little relative motion between the float and surrounding waters, perhaps the oxygen sensor spends enough time in such layers to register the local extrema. These would be very difficult for a conventional oxygen profiler to fully capture if the layers are thin since the time constant of lowered oxygen sensor is measured in seconds. That these spikes occur primarily in May suggests they are associated with, or result from, bacterial decomposition of detritus following the spring bloom.

7. Conclusions

Observation of substantial oxygen and temperature variations along outcropping float trajectories prompted us to explore the extent to which these variations could be understood in terms of biophysical processes. Using a vertical, one-dimensional model approach, we are able to recreate the observed temperature and oxygen variability for a RAFOS float that outcropped into the wintertime mixed layer of the Irminger Sea. Our model was able to predict the observed temperature to within 1°C for an entire year. The observed oxygen was also accurately reproduced by using satellite-derived observations to

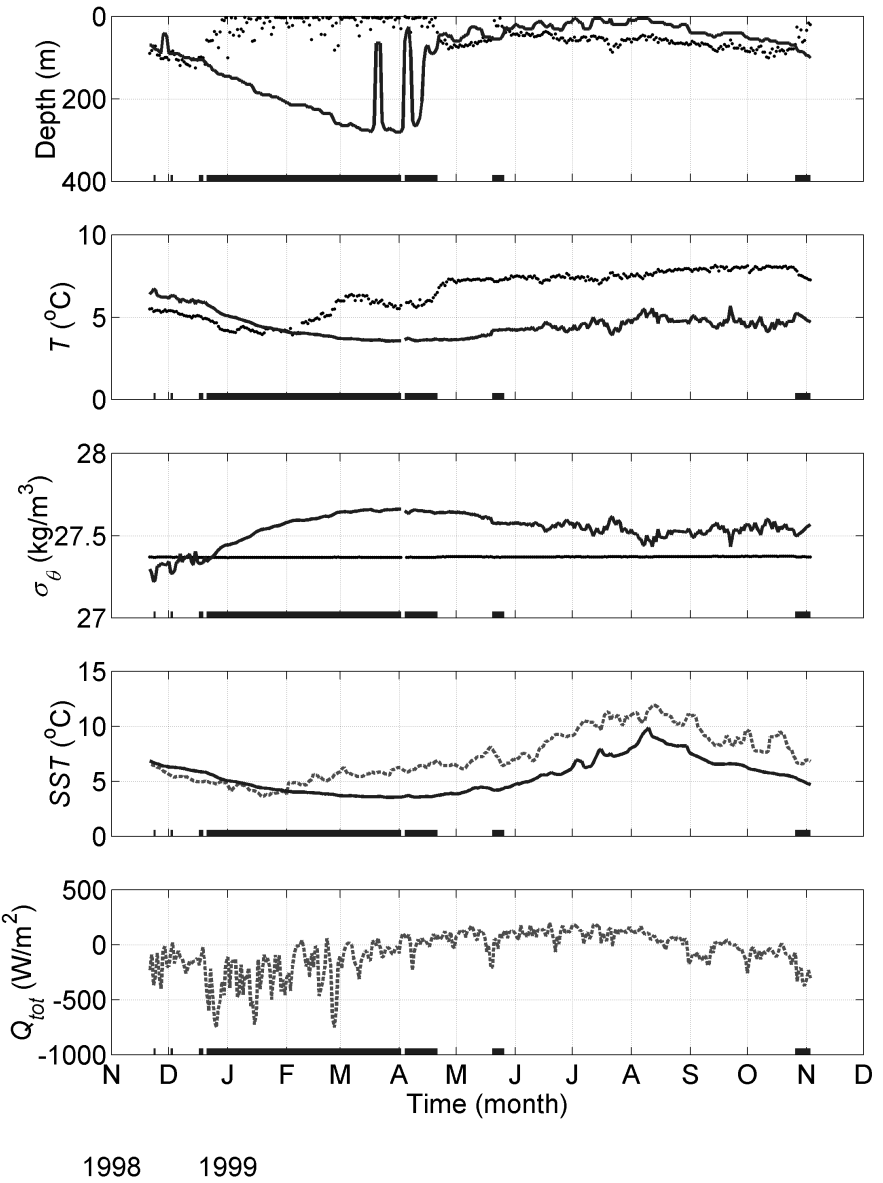

Figure 9. Model output (solid line) and float observations (dots) of pressure (depth), temperature (T), and potential density (σ_θ) for float #550. Also shown are the NCEP reanalysis products (dashed lines) of sea-surface temperature (SST) and net heat flux (Q_{tot}).

represent three major fluxes: an air-sea gas flux, oxygen production in the mixed layer via primary productivity, and oxygen consumption at depth via net community respiration. The model implicates the air-sea flux as the dominant wintertime flux, since storm activity

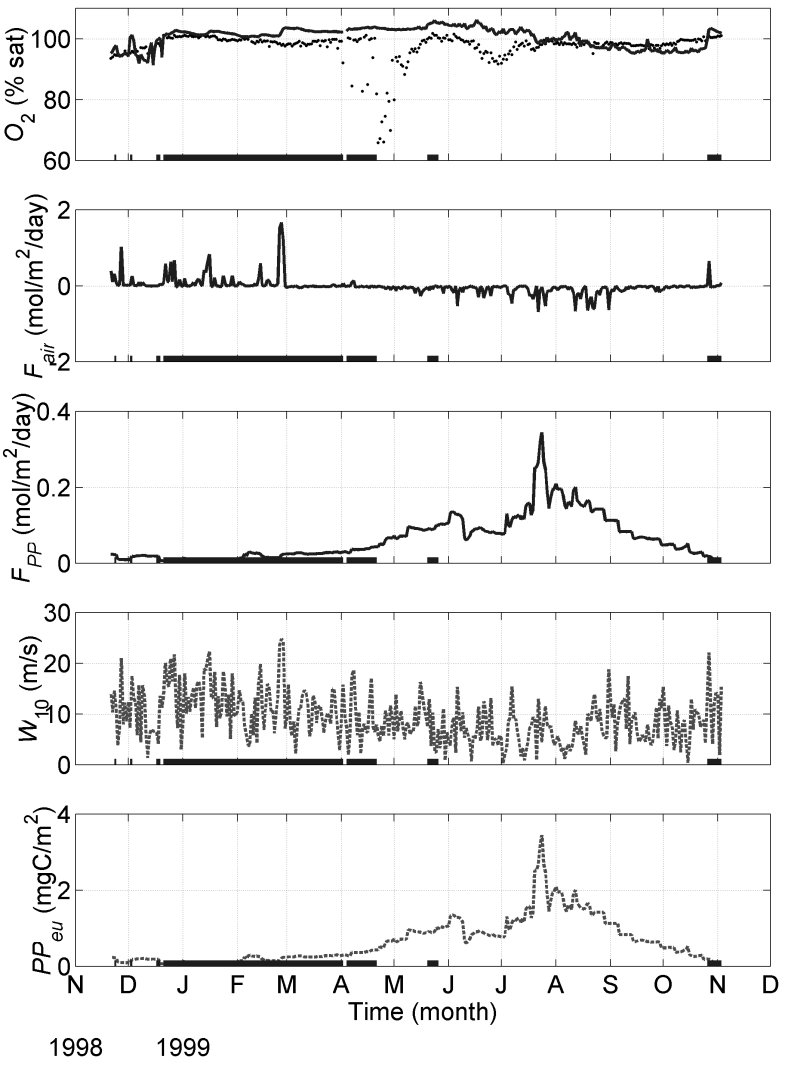

Figure 10. Model output (solid line) and float observations (dots) of oxygen (O_2) for float #550. Also shown are the modeled oxygen fluxes (F_{air} and F_{PP}). The two lower panels show the NCEP reanalysis product of the wind speed (W_{10}) and the VGPM product of primary productivity (PP_{eu}).

is high and biological activity is low, and it is able to account for the observed ~3% supersaturation in the mixed layer. Later in the year, the mixed layer stratifies during the springtime and the two biological fluxes become significant. Using an f ratio of 0.25 to estimate the net community respiration at depth, the model is able to recreate the observed oxygen drop from 105% to 92% saturation as the float subducted away from the mixed layer over a four-month period.

More generally, the results reported here indicate the power of Lagrangian techniques to probe *in situ* variability along fluid pathways. The float data reveal astonishingly large drawdowns in local oxygen in springtime. These $O(10\%)$ drawdowns are huge, albeit of short duration, probably associated with a high degree of spatial patchiness. Precisely what are the processes responsible for these large signals? There is little doubt in our minds that they are real and instrumental. It is tempting to think that these highly localized drawdowns are the first signature (or step) in the utilization of oxygen, and that these get mixed by internal waves and other diapycnal processes. On seasonal and longer time scales, can we use the observed drawdowns to make more quantitative statements about biological activity near the surface and detrital fallout at depth? Suppose floats were deployed in subtropical surface waters about to be subducted into the interior of the ocean. Can we measure the uptake of oxygen along the trajectories, and would we see variations in the rate of drawdown with the passage of the seasons as these waters are drawn deeper into the ocean? How will the rate of oxygen demand vary (decrease) with increasing depth? With the advent of new and very stable optical methods for measuring oxygen along Lagrangian pathways, it may be possible to probe the processes that govern observed distributions of oxygen in the ocean in greater detail than has been possible in the past.

Acknowledgments. We would like to thank the following members of the RAFOS float group at the Graduate School of Oceanography: Jim Fontaine, Mark Prater, Sandra Fontana, Paula Pérez-Brunius (now at Woods Hole Oceanographic Institution), and Olaf Boebel (now at AWI-Bremerhaven). Dr. Chris Langdon (Lamont-Doherty Earth Observatory, Columbia University) assisted with the technical aspects of the oxygen measurement. Mike Behrenfeld and Donal Shea (Goddard Space Flight Center, NASA) provided the VGPM data in a very timely fashion. This work was supported by NSF grants OCE-95-31878 and OCE-99-06775, and ONR/NSF grant N0001492J1651.

APPENDIX

Description of the RAFOS float

The RAFOS float is a subsurface drifter that obtains its trajectory information by listening for and determining the arrival times of acoustic signals emitted twice/day from moored sound sources at precisely known time (Rossby *et al.,* 1986). The floats also record pressure (± 5 dbar accuracy) and temperature (± 0.1°C accuracy) on the same twice/day schedule. At the end of the float's mission, typically 18 months, they surface and telemeter all data to Systeme Argos, a global radio location and data acquisition system.

The floats operate in the isopycnal mode by adding a compressible element, a compressee, that matches the float's compressibility to that of seawater. This way, the floats retain a given density surface as they change depth (Rossby *et al.,* 1985). The compressibility of the floats matched that of sea water to better than $\pm 1\%$.

Description of the oxygen sensor

Measurements of oxygen were obtained using a YSI-5750 sensor operating in the pulsed mode (Langdon, 1986). The sensor was activated for one second every 4 minutes for a total of 20 samples. The median value of the last five samples was recorded. All sensors were

calibrated at 0% and 100% saturation at two different temperatures to determine the temperature dependence of the calibration coefficients. The calibration of the sensors operating in the pulsed mode revealed almost no pressure dependence. Typical calibration accuracy in the laboratory was 5%, but some sensors showed a gradual drift after deployment. No pattern could be discerned, some were quite stable, some drifted down, and others drifted up $O(10\%)$. Comparison with hydrographic data showed no net drift when averaged over all sensors. See Lazarevich (2001) for a complete and detailed discussion of the calibration, operation, and post-mission correction to the oxygen sensors and their data.

REFERENCES

Behrenfeld, M. J. and P. G. Falkowski. 1997. Photosynthetic rates derived from satellite-based chlorophyll concentration. Limnol. Oceanogr., *42,* 1–20.

Bower, A. S., B. Le Cann, T. Rossby, W. Zenk, J. Gould, K. Speer, P. L. Richardson, M. D. Prater and H.-M. Zhang. 2002. Directly measured mid-depth circulation in the northeastern North Atlantic Ocean. Nature, *419,* 603–607.

Farmer, D. M., C. L. McNeil and B. D. Johnson. 1993. Evidence for the importance of bubbles in increasing air-sea gas flux. Nature, *361,* 620–623.

Fowler, S. W. and G. A. Knauer. 1988. Role of large particles in the transport of elements and organic compounds through the entire water column. Prog. Oceanogr., *16,* 147–194.

Kirk, J. T. O. 1983. Light and Photosynthesis in Aquatic Ecosystems, Cambridge Univ. Press, England, 401 pp.

Kistler, R., El Kalnay, W. Collins, S. Saha, G. White, J. Woollen, M. Chelliah, W. Ebisuzaki, M. Kanamitsu, V. Kousky, H. van den Dool, R. Jenne and M. Fiorino. 2001. The NCEP-NCAR 50-year reanalysis: Monthly means CD-ROM and documentation. Bull. Amer. Meteor. Soc., *82,* 247–268.

Langdon, C. 1986. Pulsing technique for improved performance of oxygen sensors. Proceedings of the Ocean 1986 Conference, Washington, D.C.

Lazarevich, P. and T. Rossby. 2001. An evaluation of the YSI-5750 oxygen sensor for use on the RAFOS float. Graduate School of Oceanography Technical Report, 2001(3), 28 pp.

Mann, K. H. and J. R. N. Lazier. 1996. Dynamics of Marine Ecosystems: Biological-Physical Interactions in the Oceans, 2nd ed., Blackwell Science, Inc., 475 pp.

Najjar, R. G. and R. F. Keeling. 1997. Analysis of the mean annual cycle of dissolved oxygen anomaly in the World Ocean. J. Mar. Res., *55,* 117–151.

——2000. Mean annual cycle of the air-sea oxygen flux: A global view. Global Biogeochem. Cycles, *14,* 573–584.

Molinari, R. L., D. Battisti, K. Bryan and J. Walsh. 1994. The Atlantic Climate Change Program. Bull. Amer. Meteor. Soc., *75,* 1191–1199.

Pérez-Brunius, P., T. Rossby and D. R. Watts. 2004. Absolute transports of mass and temperature for the North Atlantic Current-Subpolar Front system. J. Phys. Oceanogr. *34,* 1870–1883.

Plueddemann, A. J., R. A. Weller, M. Stramska, T. D. Dickey and J. Marra. 1995. Vertical structure of the upper ocean during the Marine Light-Mixed Layers experiment. J. Geophys. Res., *100,* 6605–6619.

Price, J. F., R. A. Weller and R. Pinkel. 1986. Diurnal cycling: Observations and models of the upper ocean response to diurnal heating, cooling, and wind mixing. J. Geophys. Res., *91,* 8411–8427.

Rossby, H. T., E. Levine and D. N. Conners. 1985. The isopycnal Swallow float: A simple device for tracking water parcels in the ocean. Prog. Oceanogr., *14,* 511–525.

Rossby, T., D. Dorson and J. Fontaine. 1986. The RAFOS system. J. Atmos. Oceanic Tech., *3,* 672–679.

Smayda, P. C. 1970. The suspension and sinking of phytoplankton in the sea. Oceanogr. Mar. Bio. Ann. Rev., *8,* 353–414.

Sun, C. and R. Watts. 2001. A circumpolar Gravest Empirical Model for the Southern Ocean hydrography. J. Geophys. Res., *106,* 2833–2856.

Thorpe, S. A. 1984. The role of bubbles produced by breaking waves in super-saturating the near-surface ocean mixing layer with oxygen. Ann. Geophys., *2,* 53–56.

Wallace, D. W. R. and C. D. Wirick. 1992. Large air-sea gas fluxes associated with breaking waves. Nature, *356,* 694–696.

Wanninkhof, R. and W. R. McGillis. 1999. A cubic relationship between air-sea CO_2 exchange and wind speed. Geophys. Res. Lett., *26,* 1889–1892.

Woolf, D. K. and S. A. Thorpe. 1991. Bubbles and the air-sea exchange of gases in near-saturation conditions. J. Mar. Res., *49,* 435–466.

Received: *27 May, 2003;* revised: *8 June, 2004.*